https://doi.org/10.1016/j.nanoen.2018.12.057

Three-Terminal Memtransistors Based on Two-Dimensional Layered Gallium Selenide Nanosheets for Potential Low-Power Electronics Applications

Yang Yang,[1] Huiying Du,[1] Qiang Xue,[2] Xianhua Wei,[2] Zhibin Yang,[3,4] Chenggang Xu,[1] Dunmin Lin,[1] Wenjing Jie,[1] and Jianhua Hao[3]**

[1]College of Chemistry and Materials science, Sichuan Normal University, Chengdu 610066, China.

[2]State Key Laboratory of Environment-friendly Energy Materials, Southwest University of Science and Technology, Mianyang 621010, China

[3]Department of Applied Physics, The Hong Kong Polytechnic University, Hung Hom, Kowloon, Hong Kong, China

[4]Center for Terahertz Waves and College of Precision Instrument and Optoelectronics Engineering, and the Key Laboratory of Optoelectronics Information and Technology, Ministry of Education, Tianjin University, Tianjin 300072, P. R. China

***Corresponding authors:** Wenjing Jie, Email: wenjing.jie@sicnu.edu.cn

Jianhua Hao, Email: jh.hao@polyu.edu.hk

ABSTRACT

A multi-terminal hybrid system named memtransistor has recently been proposed by combining the concepts of both memristor and field effect transistor (FET) with two-dimensional (2D) layered materials as the active semiconductor layer. In the memtransistors, the gate voltages are capable of modulating not only the transport properties of the fabricated FET, but also the resistive switching (RS) behaviors of the memristor. Herein, we employ mechanically exfoliated 2D layered GaSe nanosheets to prepare GaSe based three-terminal memtransistors. By using Ag as the electrodes, the memristor exhibits non-volatile bipolar RS characteristics. More importantly, under exposure to air for one week, the RS behaviors are dramatically enhanced with the ON/OFF ratio reaching up to 5.3×10^5 and ultralow threshold electric field of $\sim 3.3 \times 10^2$ Vcm^{-1}. The ultralow threshold electric field of GaSe based memristor could be related to the low migration energy of the intrinsic Ga vacancy in *p*-type GaSe. Moreover, the GaSe-based memristor shows long-term retention ($\sim 10^4$ s) and high cycling endurance (~5000 cycles) simultaneously. Hence, the fabricated three-terminal 2D GaSe memtransistors possess high performance with large switching ratios, ultralow threshold electric field, good endurance and long-term retention. Furthermore, the device demonstrates gate tunability in RS characteristics, suggesting the promising applications in multi-terminal electronic devices with low power consumption and complex functionalities, ranging from non-volatile memory, logic device to neuromorphic computing.

KEYWAORDS: 2D materials; GaSe; resistive switching; memristors; memtransistors

1. INTRODUCTION

Memristor has received considerable attention as the fourth fundamental passive circuit element because of its promising application in non-volatile memory, logic device and computing, owing to its low power consumption, high speed and superior scalability.[1–3] It is typically a two-terminal device with a sandwich structure of metal/resistive switching (RS) layer/metal. A large number of insulating and semiconducting materials have been reported to work as the RS materials, such as binary oxides (HfO_2,[4] TiO_x,[5] TaO_x,[6] WO_x,[7] and ZnO),[8] complex perovskite oxides and some organic materials.[9] Many strategies have been used to tune or improve the RS behaviors, such as doping,[10] structure optimization,[11] electrode and interface engineering,[12] as well as the measurement conditions.[5] Two dimensional (2D) layered materials have been widely studied ever since the first discovery of graphene by Geim's group in 2004 due to their unique structure and outstanding properties.[13,14] Recently, graphene and other 2D layered materials have also been considered as promising candidates for the fabrication of memristors. Graphene can be used as an electrode or an interface layer between the electrode and dielectric to block atomic diffusion and limit the number of conductive filaments.[15,16] In addition, various RS behaviors have been reported in a series of 2D materials,[17,18] including graphene oxide,[19] transition metal dichalcogenides (TMDs),[20,21] hexagonal boron nitride[22] and black phosphorous.[23] In comparison with traditional oxide-based RS devices, memristors based on 2D layered materials not only provide 2D devices platform for memory but also have potential to work at relatively low operating voltages, suggesting promising applications in energy-efficient memristor-based neural networks.[21,24] Among 2D materials, MoS_2-based memristors have been intensively investigated recently. A robust memristor based on heterostructure of graphene/MoS_2/graphene

demonstrated good thermal stability in a broad temperature range of 20~340℃.[25] In 2015, RS behaviors were achieved in monolayer MoS_2 based field effect transistors (FETs) through modulating the grain boundary.[26] The third terminal applied gate voltage can tune the set voltage from 3.5 to 8.0 V by utilizing the field-effect geometry. Recently, Sangwan *et al*. proposed the concept of memtransistor which is a multi-terminal device combining the characteristics of a memristor and a transistor based on polycrystalline monolayer MoS_2.[27] In the memtransistors, the gate voltages are capable of modulating not only the transport properties of the fabricated FET, but also the RS characteristics of the memristor. Based on the 2D monolayers, the memtransistor operates much like a neuron by performing both memory and information processing.

Beyond TMDs, 2D layered III-VI semiconducting materials have drawn much attention due to their fascinating electrical and optical properties.[28] Among them, gallium selenide (GaSe) is an *p*-type semiconductor with an indirect band gap of ~2.0 eV and a direct band gap of only ~25 meV or above.[29] In its 2D forms, GaSe is expected to have excellent optical and electrical properties,[30–32] suggesting promising applications in nonlinear optics, terahertz generation and optoelectronics.[33–35] Thus, it is meaningful to investigate the intriguing 2D layered material in memristors for multi-functional devices to perform complex functions in 2D platform by utilizing its electrical and optical advantages. Furthermore, it is essential to explore new 2D materials for applications in RS devices from the point of view in materials science. However, until now, the use of 2D layered GaSe has not been reported in memristors or memtransistors. In this work, mechanically exfoliated 2D layered GaSe nanosheets have been employed to serve as the RS layer in the memristor device. Based on the FET structure, a memtransistor has been fabricated by using gate voltage to achieve three-terminal device. This provides us opportunity to

explore the energy-efficient multi-terminal devices and analyze the underlying physical mechanism based on 2D GaSe nanosheets.

2. METHODS

Fabrication of GaSe-based memtransistors: 2D layered GaSe nanosheets were prepared by mechanical exfoliation method.[30] After the GaSe flakes were transferred onto the 300-nm SiO_2 coated Si substrates, Ag electrodes were fabricated with using a stripe mask by using sputtering method. The thickness of electrodes is well controlled to be ~100 nm and the distance between the adjacent electrodes is ~30 μm. The adjacent electrodes and the underlying GaSe nanosheets can form metal-semiconductor-metal (M-S-M) configuration for RS measurements. At the same time, FET structure can be constructed with the adjacent electrodes serving as the source and drain electrodes, the Si working as the gate electrode and the SiO_2 as gate insulator. Figure 1a shows a schematic of the Ag/GaSe/Ag memtransistor with horizontal electrode geometry by combining the concept of memristor and the FET structures. Thus, the multi-terminal memtransistor can be constructed by combining memristor and the FET based on 2D GaSe nanosheets.

Characterizations: Atomic force microscope (AFM, DI Nanocope 8) was employed to characterize the surface morphology and determine the thickness of the exfoliated GaSe nanosheets. Besides, the exfoliated GaSe flakes were characterized using Raman spectroscopy (HORIBA JOBIN YVON, HR800) with the excitation wavelength of 633 nm and a spot size of ~1 μm. All the RS behaviors and transport properties were measured by double channel Keithley 2636B SourceMeter with a four-probe station system. All measurements were performed under air ambient at room temperature.

3. RESULTS AND DISCUSSION

Figure 1b exhibits the crystal structure of GaSe with two layers of Se respectively in the top and the bottom and two layers of Ga ions in the middle. The covalently bonded basic layers are stacked together by a weak van der Waals interaction to form GaSe crystal.[36,37] Figure 1c shows the atomic force microscopy (AFM) image of the mechanically exfoliated GaSe nanosheet. The AFM height profile is shown in the bottom inset of Figure 1c, suggesting the exfoliated GaSe nanosheet with layer number of ~10. The inset of top panel in Figure 1c demonstrates the optical image of the GaSe nanosheet on SiO_2/Si substrate, suggesting a well exfoliated flake for device fabrication. This flake was used as the channel material to connect the source and drain electrode with the FET structure, as schematically shown in Figure 1a. The FET channel length, determined by the FET structure, is ~30 μm. Figure 1d shows the typical Raman spectrum of multilayer GaSe flake. Two Raman feature peaks, located at 135 cm^{-1} and 308 cm^{-1}, can be clearly observed, corresponding to the two out-of-plane modes of A^1_{1g} and A^2_{1g}, respectively. In addition, two weak peaks in the Raman spectrum are the in-plane vibrational modes of E^2_{1g} (250 cm^{-1}) and E^1_{2g} (212 cm^{-1}). All these Raman feature peaks agree well with previously reported exfoliated GaSe nanosheets.[37]

The RS behaviors of GaSe based memristor are measured at room temperature. Figure 2a shows a typical current–voltage (*I–V*) curve of the fabricated Ag/GaSe/Ag memristor with the operating voltage of 2 V without an electroforming process. The device exhibits bipolar RS behaviors and no additional forming process is further required. In our experiment, the bias voltage is scanned in the sequence of 0 V→+2 V→0 V→–2 V→0 V. The arrows suggest the scanning direction of the bias voltage. A positive voltage of about 1V can switch the memory device from the high

resistance state (HRS) (*i.e.* OFF state) to the low resistance state (LRS) (*i.e.* ON state), which is defined as a set process (process 1). Accordingly, the SET voltage (V_{SET}) is 1 V for the memristor. Although the V_{SET} is not very low, the corresponding set electric field (E_{SET}) is ultralow (~3.3×10^2 V cm^{-1}) by considering the lateral RS device with the channel length of 30 μm.[38,39] The LRS remains unchanged during subsequent voltage sweeps (process 2&3), suggesting the nonvolatile nature of the memory device. On the other hand, a negative bias (~ –1 V) can returns the device to the OFF state, which is called the reset process. The memristor device exhibits a bipolar switching mode with an ON/OFF ratio up to 1.16×10^3. It should be noted that the RS properties do not show remarkable changes in the set and reset voltages from the initial bias scan loop, as shown in Figure 2b. The GaSe-based memristor exhibits repeatable resistive switching cycles, suggesting a high degree of stability.

In order to clearly explore the physical mechanism of the bipolar RS behaviors, the positive part of *I–V* curve in Figure 2a is re-plotted using double-logarithmic coordinates, as shown in Figure 2c. The *I–V* curve of the HRS follows a quadratic behavior ($I \sim V^2$) at low voltage (V <1 V) with the addition of $I \sim V^a$ (a > 2) at higher voltage (V > 1 V), which is typical space charge limited current (SCLC) injection. Moreover, the *I–V* relationship follows Ohmic conduction (I~V) in the whole LRS. To further understand the observed switching behaviors, we should carefully analyze the electric band structure for GaSe and Ag. The electron affinity of GaSe (χ_{GaSe}) is ~3.1 eV and the ionization energy (E_{ion}) is ~5.1 with the bandgap of about 2 eV.[40] The work function (Φ) of Ag is 4.26. The band diagram for metal/semiconductor (M/S) junction of Ag/GaSe is shown in Figure 2d. Theoretically, Schottky junction can be formed when *p*-type semiconductor with electron affinity higher than the work function of the metal (Ag) with Schottky-barrier height ($\Phi_b = \chi_{GaSe} - \Phi_{Ag}$). Accordingly, a space-charge region is formed

accompanied by the build-in voltage (V_i) in the semiconductor near the interface with potential of $eV_i = \Phi_{\text{p-GaSe}} - \Phi_{\text{Ag}}$. The Schottky barrier formed between the electrodes and the GaSe nanosheets plays an important role in the resistance.[41] To be more specific, 2D layered GaSe is intrinsic *p*-type with the carrier of the Ga vacancy.[31,32] The intrinsic Ga vacancies can serve as atom-level traps. At the initial state, the device is in the HRS due to the large contact resistance between GaSe and Ag. When a forward bias is applied, electrons are captured and filled into traps until they are saturated and then emitted from the fermi level to the conduction band. The vacancy migration will be able to modulate the Schottky barrier,[42–44] inducing the Ohmic contact between the Ag electrode and the 2D GaSe nanosheet. The device is switched from the HRS to the LRS, corresponding to the set process in the GaSe memristor. The electronic resistive switching memory behaviors were also observed in one-dimensional selenide microwires with the lateral Ag/$MoSe_2$-deped Se/Ag memory devices.[45]

Moreover, Ag electrode, as the active metallic, has the potential to form metal conductive filaments and switch the device from the HRS to the LRS.[10] In this case, the electrochemical metallization (ECM) can be employed to explain RS behaviors.[46] However, the memristors with ECM usually have an electrochemically active electrode, such as Ag or Cu, and an electrochemically insert metal, such as Pt or Au. In our experiments, the symmetric Ag electrodes are used. Thus, the Ag filament is unlikely to form in the LRS. Moreover, it is reported that Ag migration resistive switching memories typically require much higher electric fields for SET (>1×10^5 V cm^{-1}),[4] while, ultralow electric filed (~10^2 V cm^{-1}) is needed in 2D GaSe-based memristor. By considering the ultralow electrical field, the Ag filament is unlikely to be formed in the fabricated GaSe memristors. Besides, we prepared an inert Au electrode to construct lateral memristors. A typical rectifying resistive switching can be clearly detected with

on/off ratio of 4×10^3 (not shown here). This result can further rule out the possibility of forming Ag filament in 2D GaSe based memristors. However, the switching mechanism in 2D layered materials may be relevant to a complex competition among several parameters including grain size, lateral area, and the interface between electrodes and active layer.[17] Actually, it would be better to compare lateral memristors with different channel lengths. However, it is very difficult for us to fabricate the memory devices with channel length less than 10 μm by using photolithography since the chemical solutions used in photolithography could dramatically destroyed GaSe nanosheets. Thus, we are trying to fabricate large-area GaSe flakes by chemical vapor deposition method.

Next, it is very intriguing to observe that the RS behaviors are enhanced dramatically when the memristors are stored in a dry box for more than one week. The stored device is marked as memristor# for convenience. An electroforming process with forming voltage of –3 V is necessary for the memristor# before it exhibited the resistive switching behaviors. Initially, the Ag memristor# is in the LRS due to the previous electroforming process, as shown in Figure 3a. Then, the device suddenly changes to HRS when the applied voltage is increased to 1.5 V in process 1, suggesting the reset process with the reset voltage (V_{RESET}) of 1.5 V. The HRS is maintained during the entire process 2 from 2 to 0 V. Subsequently, the HRS is changed into the LRS biased by the negative voltage in excess of –1 V in process 3 and the LRS remains unchanged during the overall process 4. The Ag memristor# exhibits excellent RS behaviors with a high ON/OFF current ratio up to 5.3×10^5. Therefore, our device exhibits comparable RS behaviors to traditional oxide thin film resistor devices, and more importantly, the corresponding E_{SET} is ultralow with the magnitude of $\sim3.3 \times 10^2$ V cm^{-1}.[38] When compared to previously reported 2D materials based memristors, our GaSe based devices not only possess high ON/OFF

current ratio and comparable V_{SET} to some vertical devices,[17] but also exhibit lower V_{SET} and E_{SET} to some lateral devices.[26,27] For example, MoS_2 based lateral memristors usually have high operation voltage of ~10 V and even higher value.[21,26,27] While, our lateral devices work at relative low operation voltage of 2 V. The ultralow E_{SET} of GaSe based memristor could be related to the low migration energy of Ga vacancy. 2D layered GaSe is more favorable to creating Ga vacancy, inducing the intrinsic *p*-type properties.[47] It was reported that Ga vacancy can migrate with low activation energy less than 0.2 eV according to the first-principles calculations.[48] This value is significantly smaller than the migration energy of oxygen vacancy (1.15 eV) which is the dominating charge carrier in resistive switching devices where a much higher set field of about 10^5 V cm^{-1} is required to achieve RS.[49] Therefore, the GaSe-based memristor# not only possesses a high ON/OFF current ratio, but also shows ultralow E_{SET}, suggesting the potential of real applications in low-power nonvolatile memory. Furthermore, the Ag memristor# exhibits good repeatability with 50 experimental switching loops of *I–V* curves, as shown in Figure 3b.

The RS behaviors of memristor# is dramatically improved compared with its fresh device. A clear switching mechanism is critical to the understand the unique RS performance. Firstly, the positive part of *I–V* curve in Figure 3a is re-plotted using double-logarithmic coordinates, as shown in Figure 3c. For the LRS, the slope is 1.05, indicating the initial ohmic contact between Ag and GaSe for the memristor#. For the HRS, two distinguished regions with slopes both much larger than 1 (4.74 and 2.23, respectively) can be observed in the linear fitted *I–V* characteristics. To further understand the electrical properties of GaSe, the transport properties of 2D GaSe-based FETs of as-fabricated and under one-week exposure to air are studied, as shown in Figure 3d. The drain voltage (V_{ds}) is set to be 0.8 V. Both devices show a typical *p*-type transport

behavior with the gate voltage (V_g) swept from –20 to 20 V. The transport curve of GaSe# shows a right shift compared to the GaSe curve, indicating the GaSe becomes more *p*-type after being exposured to air for a period. 2D layered GaSe nanosheets are not stable under ambient conditions, giving rise to high density charged traps.[50,51] In this case, Ga vacancy can form conductive filaments under external forming electric field, inducing the Ohmic conduction behavior in LRS. In the *p*-type GaSe, there are some mobile Se ions near the Ga vacancies, as shown in Figure 4a. When a negative V_{ds} is applied, Se ions can migrate toward the source electrode. Then the accumulated Se ions can generate cation vacancies at the interface between the Ag electrode and the GaSe, as schematically shown in Figure 4b. The Ga vacancies can serve as the nuclei of *p*-type conductive filaments. When the negative voltage increases, the nuclei can grow up under the electric field until the conductive filament is formed. At this stage, the device is switched into LRS, i.e., the SET process, as demonstrated in Figure 4c. When a positive V_{ds} is applied, Se ions can migrate toward the drain electrode under electric field, inducing the break of the Ga vacancy filament, i.e., the RESET process (Figure 4d).

Moreover, the data retention and device endurance were tested in pulse mode in order to evaluate the potential applications in nonvolatile memory. Figure 5a shows the data retention of the Ag memristor# at room temperature. The voltage pulses with a 0.1 s pulse duration are applied with 1.5 V magnitude as V_{RESET} and –1 V as V_{SET}, respectively. The read voltages are 1 and –0.5 V for HRS and LRS, respectively. The currents for both HRS and LRS are slightly increased with time, but the device kept the high ON/OFF ratio of more than 10^3 for 10^4 s. Figure 5b shows endurance test based on Ag memristor# at room temperature. The resistances of both HRS and LRS show a slight and monotonical decreasing trend with cycle number. The resistance ratio of HRS and LRS can reach up to 10^3 for 5000 cycles, suggesting excellent stability for the

memristor working continuously in the pulse mode. However, it is difficult for us to measure the speed of switching at current stage by considering the setup limits. Next, we will focus on the ultrafast measurements of the GaSe-based memristors for potential low-power electronics applications.

Furthermore, the three-terminal memristors can be achieved based on the FET configuration, providing us opportunities for future low-power applications in memristive circuits and related multi-terminal devices. The RS behaviors are measured based on the three-terminal device during the applied V_g. As shown in Figure 6a, the current level of both LRS and HRS remain almost constant with the unchanged ON/OFF ratio when the V_g is applied from 20 to –20 V. Only the gate-dependent SET and RESET voltages can be achieved in our experiments. To understand the abnormal behaviors, the transport properties of GaSe FETs at HRS and LRS are studied, as shown in Figure 6b. The drain voltage (V_{ds}) is –2 V and 2 V for LRS and HRS respectively. At HRS, the FET shows the ON/OFF ratio of ~100, while only ON/OFF ratio of ~8 can be achieved for LRS when the V_g is swept from –20 to 20 V. On the other hand, the 2D GaSe nanosheets used for both fresh and stored FETs demonstrate the ON/OFF ratio of ~1000 with the V_{ds} of 0.8 V before the RS measurements. The experimental data suggest that the field effects on the currents are weakened at both HRS and LRS. It is known that the V_g can tune the carrier density of 2D materials through the applied electric field. Thus, the additional carriers provided by the external field play a major role in the SET voltage. The absence of the gate tuning of current has been reported in lateral memristors based on monolayer MoS_2 with intersecting grain boundary.[26] The V_{SET} is gradually changed from –1.3 to –0.5 V though changing V_g from 20 to –20 V. To be more specific, a positive V_g can evidently reduce the V_{RESET}, while a negative one shows slight effects on the V_{RESET}. In general, a negative V_g can significantly reduce the

V_{SET}, while the V_{RESET} remains almost unchanged. On the other hand, a positive V_g can reduce the V_{RESET} and increase the V_{SET}, inducing the left shift of the switching window. When the V_g is applied, the carrier density in GaSe nanosheets can be tuned through the field effect. A negative V_g can provide the doping carriers, which may contribute to the conduction of GaSe, inducing a decreased V_{SET}, while, a positive V_g gives rise to the decrease in carrier density in GaSe, resulting an increased V_{SET}. Therefore, GaSe based memtransistors not only possess large switching ratios, ultralow E_{SET}, good endurance and long-term retention, but also demonstrate gate tunability in RS properties.

In conclusions, we have successfully demonstrated three-terminal memtransistors based on mechanically exfoliated 2D layered GaSe nanosheets through combing the devices of a memristor and a FET. This work can enlarge the family of RS materials and show more new characteristics which have not previously addressed. The GaSe-based memristor exhibits non-volatile bipolar RS behaviors. Under exposure to air for one week, the RS behaviors are dramatically enhanced with the ON/OFF ratio reaching up to 5.3×10^5 and the ultralow set and reset electric fields of $\sim 3.3 \times 10^2$ Vcm^{-1}. The ultralow E_{SET} of GaSe based memristor could be related to the low migration energy of the intrinsic Ga vacancy in *p*-type GaSe, implying the potential of real applications in low-power nonvolatile memories. Furthermore, the V_g not only can tune the transport characteristics of GaSe-based FETs, but also adjust the V_{SET} and V_{RESET} in GaSe based memristors, suggesting the promising applications in multi-terminal electronic devices with low power consumption and complex functionalities.

ACKNOWLEDGEMENT

This work was supported by the grants from National Natural Science Foundation of China (No. 61604100 & No. 51772252) and Hong Kong RGC GRF (PolyU 153033/17P).

REFERENCES

[1] P.H. Liu, C.C. Lin, A. Manekkathodi, L.J. Chen, Nano Energy. 15 (2015) 362–368.

[2] C.F. Kang, W.C. Kuo, W. Bao, C.H. Ho, C.W. Huang, W.W. Wu, Y.H. Chu, J.Y. Juang, S.H. Tseng, L. Hu, J.H. He, Nano Energy. 13 (2015) 283–290.

[3] C.H. Chiu, C.W. Huang, Y.H. Hsieh, J.Y. Chen, C.F. Chang, Y.H. Chu, W.W. Wu, Nano Energy. 34 (2017) 103–110.

[4] R. Waser, R. Dittmann, G. Staikov, K. Szot, Adv. Mater. 21 (2009) 2632–2663.

[5] G. Zhou, S. Duan, P. Li, B. Sun, B. Wu, Y. Yao, X. Yang, J. Han, J. Wu, G. Wang, L. Liao, C. Lin, W. Hu, C. Xu, D. Liu, T. Chen, L. Chen, A. Zhou, Q. Song, Adv. Electron. Mater. 4 (2018) 1700567.

[6] C.F. Chang, J.Y. Chen, G.M. Huang, T.Y. Lin, K.L. Tai, C.Y. Huang, P.H. Yeh, W.W. Wu, Nano Energy. 53 (2018) 871–879.

[7] S. Lee, J. Lee, J. Park, Y. Choi, K. Yong, Adv. Mater. 24 (2012) 2418–2423.

[8] W.-Y. Chang, Y.-C. Lai, T.-B. Wu, S.-F. Wang, F. Chen, M.-J. Tsai, Appl. Phys. Lett. 92 (2008) 22110.

[9] H. Wang, Y. Du, Y. Li, B. Zhu, W.R. Leow, Y. Li, J. Pan, T. Wu, X. Chen, Adv. Funct. Mater. 25 (2015) 3825–3831.

[10] F. Pan, S. Gao, C. Chen, C. Song, F. Zeng, Mater. Sci. Eng. R Reports. 83 (2014) 1–59.

[11] E. Linn, R. Rosezin, C. Kügeler, R. Waser, Nat. Mater. 9 (2010) 403–406.

[12] S.K. Kim, J.Y. Kim, S.Y. Choi, J.Y. Lee, H.Y. Jeong, Adv. Funct. Mater. 25 (2015) 6710–6715.

[13] W. Jie, Z. Yang, G. Bai, J. Hao, Adv. Opt. Mater. (2018) 1701296.

[14] W. Jie, J. Hao, Nanoscale. 6 (2014) 6346–6362.

[15] S. Liu, N. Lu, X. Zhao, H. Xu, W. Banerjee, H. Lv, S. Long, Q. Li, Q. Liu, M. Liu, Adv. Mater. 28 (2016) 10623–10629.

[16] J. Yao, J. Lin, Y. Dai, G. Ruan, Z. Yan, L. Li, L. Zhong, D. Natelson, J.M. Tour, Nat. Commun. 3 (2012) 1101.

[17] R. Ge, X. Wu, M. Kim, J. Shi, S. Sonde, L. Tao, Y. Zhang, J.C. Lee, D. Akinwande, Nano Lett. 18 (2018) 434–441.

[18] M. Kim, R. Ge, X. Wu, X. Lan, J. Tice, J.C. Lee, D. Akinwande, Nat. Commun. 9 (2018) 1–7.

[19] F. Zhao, L. Wang, Y. Zhao, L. Qu, L. Dai, Adv. Mater. 29 (2017) 1604972.

[20] P. Cheng, K. Sun, Y.H. Hu, Nano Lett. 16 (2016) 572–576.

[21] D. Li, B. Wu, X. Zhu, J. Wang, B. Ryu, W.D. Lu, X. Liang, ACS Nano. 12 (2018) 9240–9252.

[22] K. Qian, R.Y. Tay, V.C. Nguyen, J. Wang, G. Cai, T. Chen, E.H.T. Teo, P.S. Lee, Adv. Funct. Mater. 26 (2016) 2176–2184.

[23] Y. Cao, X. Tian, J. Gu, B. Liu, B. Zhang, S. Song, F. Fan, Y. Chen, Angew. Chemie Int. Ed. 57 (2018) 4543–4548.

[24] A.A. Bessonov, M.N. Kirikova, D.I. Petukhov, M. Allen, T. Ryhänen, M.J.A. Bailey, Nat. Mater. 14 (2015) 199–204.

[25] M. Wang, S. Cai, C. Pan, C. Wang, X. Lian, Y. Zhuo, K. Xu, T. Cao, X. Pan, B. Wang, S.-J. Liang, J.J. Yang, P. Wang, F. Miao, Nat. Electron. 1 (2018) 130–136.

[26] V.K. Sangwan, D. Jariwala, I.S. Kim, K.-S. Chen, T.J. Marks, L.J. Lauhon, M.C. Hersam, Nat. Nanotechnol. 10 (2015) 403.

[27] V.K. Sangwan, H.-S. Lee, H. Bergeron, I. Balla, M.E. Beck, K.-S. Chen, M.C. Hersam, Nature. 554 (2018) 500.

[28] Z. Yang, W. Jie, C.-H. Mak, S. Lin, H. Lin, X. Yang, F. Yan, S.P. Lau, J. Hao, ACS Nano. 11 (2017) 4225–4236.

[29] Y. Fan, M. Bauer, L. Kador, K.R. Allakhverdiev, E.Y. Salaev, J. Appl. Phys. 91 (2002) 1081–1086.

[30] W. Jie, X. Chen, D. Li, L. Xie, Y.Y. Hui, S.P. Lau, X. Cui, J. Hao, Angew. Chem. Int. Ed. 54 (2015) 1185–1189.

[31] P. Hu, Z. Wen, L. Wang, P. Tan, K. Xiao, ACS Nano. 6 (2012) 5988–5994.

[32] D.J. Late, B. Liu, J. Luo, A. Yan, H.S.S.R. Matte, M. Grayson, C.N.R. Rao, V.P. Dravid, Adv. Mater. 24 (2012) 3549–3554.

[33] X. Zhou, J. Cheng, Y. Zhou, T. Cao, H. Hong, Z. Liao, S. Wu, H. Peng, K. Liu, D. Yu, J. Am. Chem. Soc. 137 (2015) 7994–7997.

[34] Y. Zhou, Y. Nie, Y. Liu, K. Yan, J. Hong, C. Jin, Y. Zhou, J. Yin, Z. Liu, H. Peng, ACS Nano. 8 (2014) 1485–1490.

[35] M. Mahjouri-Samani, R. Gresback, M. Tian, K. Wang, A.A. Puretzky, C.M. Rouleau, G. Eres, I.N. Ivanov, K. Xiao, M.A. McGuire, G. Duscher, D.B. Geohegan, Adv. Funct. Mater. (2014) 6365-6371.

[36] L. Plucinski, R. Johnson, B. Kowalski, K. Kopalko, B. Orlowski, Z. Kovalyuk, G. Lashkarev, Phys. Rev. B. 68 (2003) 125304.

[37] D.J. Late, B. Liu, H.S.S.R. Matte, C.N.R. Rao, V.P. Dravid, Adv. Funct. Mater. 22 (2012) 1894–1905.

[38] J. Choi, S. Park, J. Lee, K. Hong, D.H. Kim, C.W. Moon, G. Do Park, J. Suh, J. Hwang, S.Y. Kim, H.S. Jung, N.G. Park, S. Han, K.T. Nam, H.W. Jang, Adv. Mater. 28 (2016) 6562–6567.

[39] F. Zhou, Y. Liu, X. Shen, M. Wang, F. Yuan, Y. Chai, Adv. Funct. Mater. 28 (2018) 1800080.

[40] R. Schlaf, O. Lang, C. Pettenkofer, W. Jaegermann, J. Appl. Phys. 85 (1999) 2732–2753.

[41] A. Sawa, Mater. Today. 11 (2008) 28–36.

[42] Y. Cui, H. Peng, S. Wu, R. Wang, T. Wu, ACS Appl. Mater. Interfaces. 5 (2013) 1213–1217.

[43] X. Guan, W. Hu, M.A. Haque, N. Wei, Z. Liu, A. Chen, T. Wu, Adv. Funct. Mater. 28 (2018) 1704665.

[44] S. Wu, X. Luo, S. Turner, H. Peng, W. Lin, J. Ding, A. David, B. Wang, G. Van Tendeloo, J. Wang, T. Wu, Phys. Rev. X. 3 (2013) 41027.

[45] G. Zhou, B. Sun, Y. Yao, H. Zhang, A. Zhou, K. Alameh, B. Ding, Q. Song, Appl. Phys. Lett. 109 (2016) 143904.

[46] I. Valov, R. Waser, J.R. Jameson, M.N. Kozicki, Nanotechnology. 22 (2011) 289502.

[47] S. Wu, X. Dai, H. Yu, H. Fan, J. Hu, W. Yao, (2014) arXiv:1409.4733.

[48] T. Angsten, T. Mayeshiba, H. Wu, D. Morgan, New J. Phys. 16 (2014) 15018.

[49] Z. Zhang, Q. Ge, S.C. Li, B.D. Kay, J.M. White, Z. Dohnálek, Phys. Rev. Lett. 99 (2007) 126105.

[50] J.Y. Tan, A. Avsar, J. Balakrishnan, G.K.W. Koon, T. Taychatanapat, Appl. Phys. Lett. 104 (2014) 183504.

[51] A.K. Geim, I. V. Grigorieva, Nature. 499 (2013) 419–425.

Figures

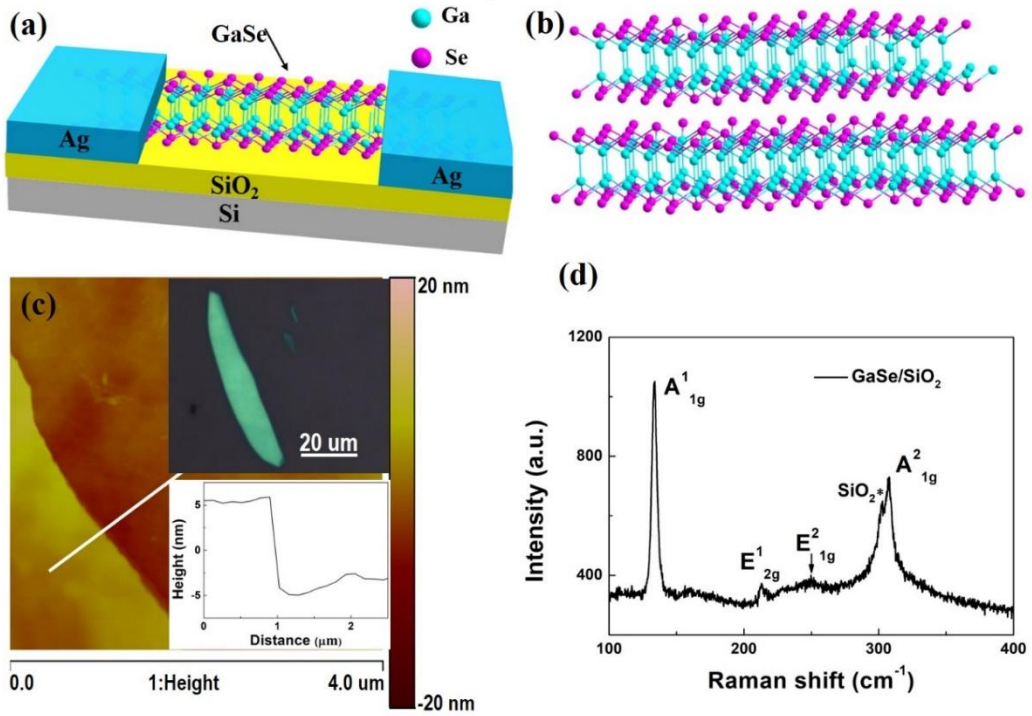

Figure 1. (a) Schematic of the 2D GaSe based memristor with the FET structure. (b) The schematic of the atomic structure of GaSe. (c) The AFM image of the exfoliated the GaSe nanosheet. Bottom panel inset: AFM height profile corresponding to the while line in the main image. Top panel inset: optical image of the exfoliated GaSe nanosheet. (d) Raman spectrum of the GaSe sample on SiO_2 substrate. The peak with * located around 305 cm^{-1} corresponds to the Raman feature mode of SiO_2.

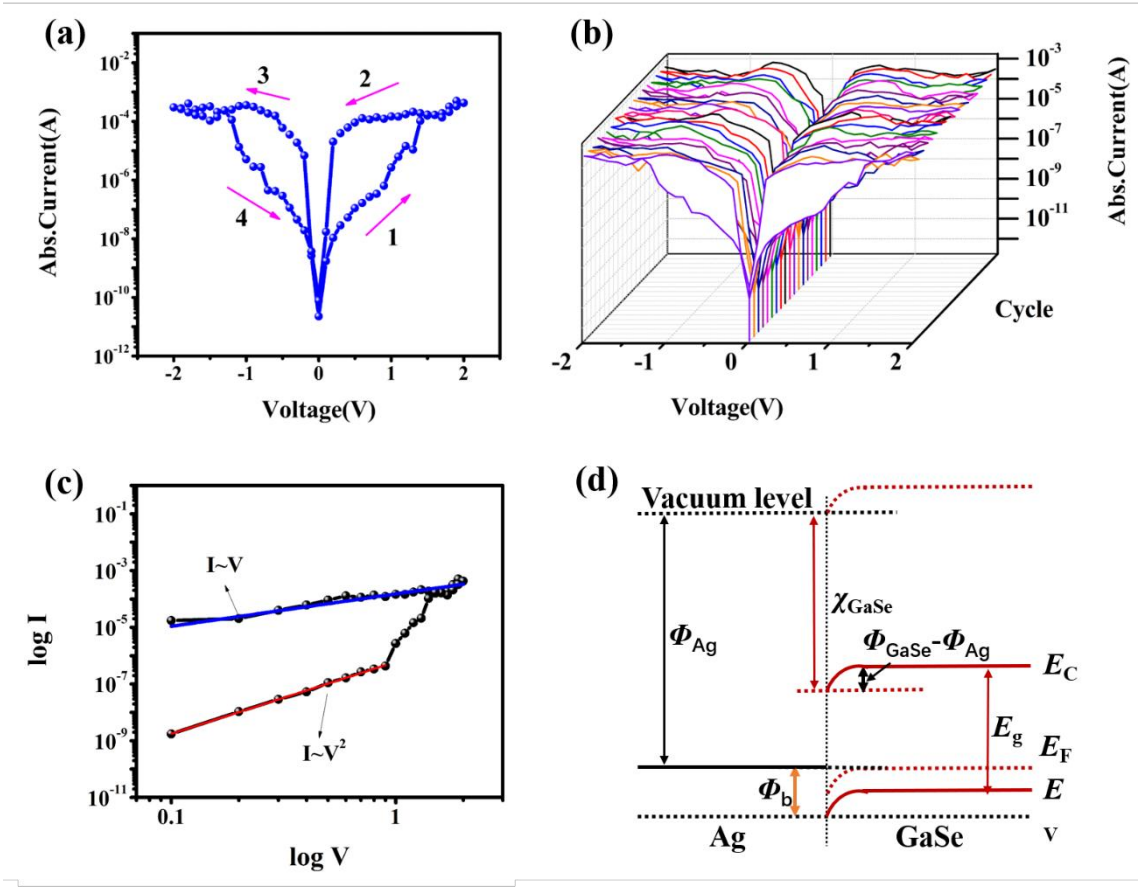

Figure 2. Resistive switching behaviors of the GaSe-based memristor. The switching directions are shown by the arrows. (a) $I-V$ characteristics of the Ag/GaSe/Ag memristor at the operating voltage of 2V. (b) 50 experimental switching loops of the Ag/GaSe/Ag memristor. (c) The positive part of the $I-V$ curve in (a) is re-plotted in a double-logarithmic coordinate and linear fitting of log(I)−log(V) curve. (d) The band diagram for metal-semiconductor junction of Ag/GaSe. E_C, E_V, E_F correspond to the conduction band edge, valence band edge, and Fermi level of p-GaSe, respectively. E_g stands for the energy gap.

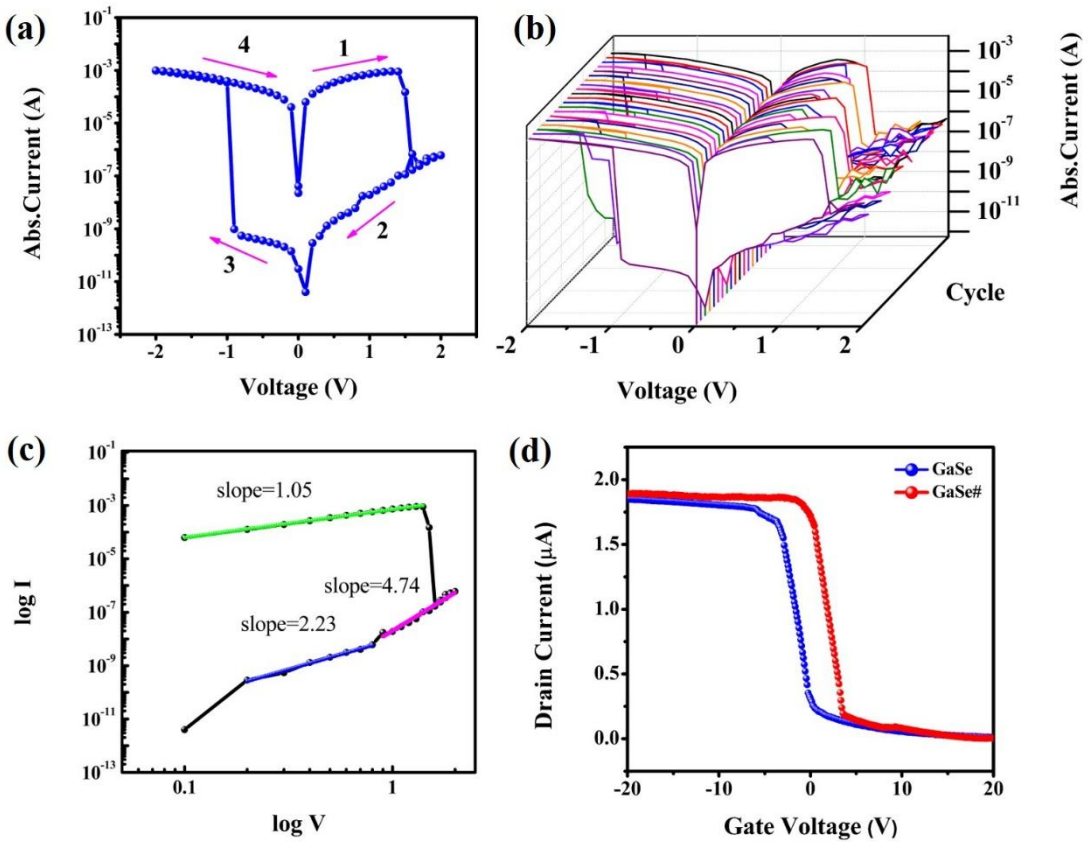

Figure 3. Resistive switching behaviors of the GaSe-based memristor after being stored in air for one week. The switching directions are denoted by the arrows. (a) $I-V$ characteristics of the GaSe memritor# at the operating voltage of 2V. (b) 50 experimental switching loops of the GaSe memristor#. (c) The positive part of the $I-V$ curve in (a) is re-plotted in a double-logarithmic coordinate and linear fitting of $\log(I)-\log(V)$ curve. (d) Transport characteristics of as-fabricated 2D GaSe-based FETs and the device under one-week exposure in air

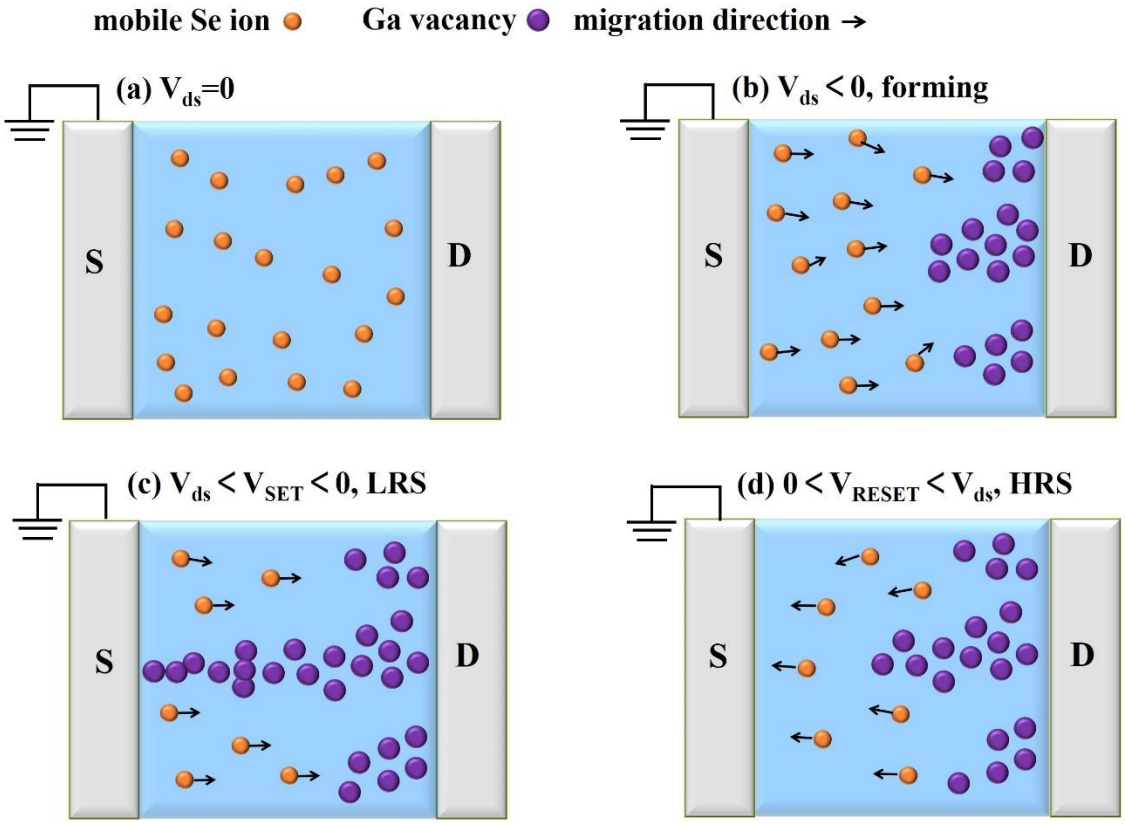

Figure 4. Schematic the RS mechanism for GaSe memristor#. (a) The initial state with the V_{ds} = 0. (b) The nucleation and growth of conductive filaments of Ga vacancies. (c) The LRS with the filaments connecting the source and drain electrodes. (d) The HRS with the broken filaments.

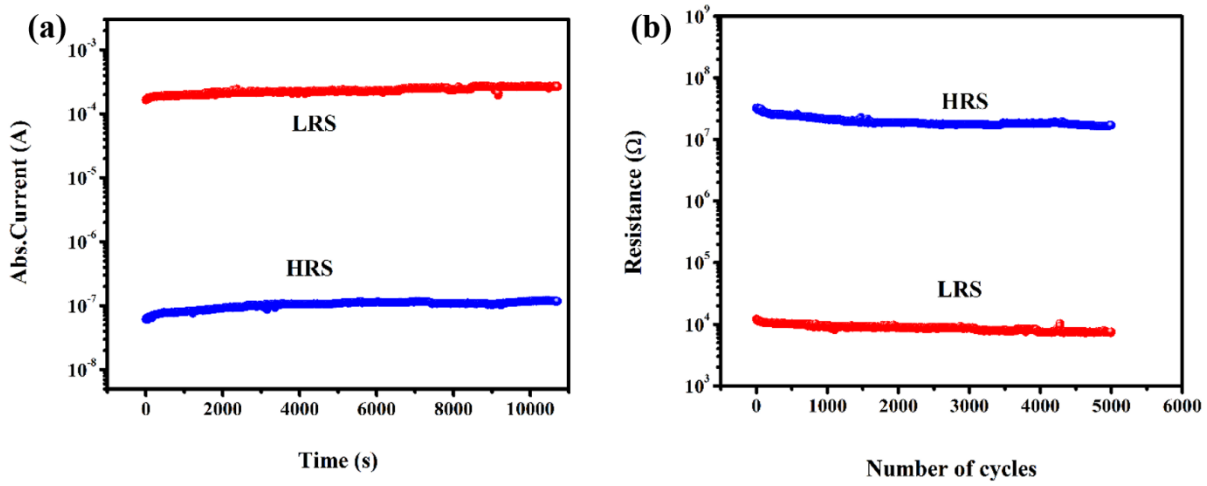

Figure 5. (a) Switching cycles of Ag/GaSe/Ag memeristor# measured with voltage pulses. (b) Switching endurance of the memory device.

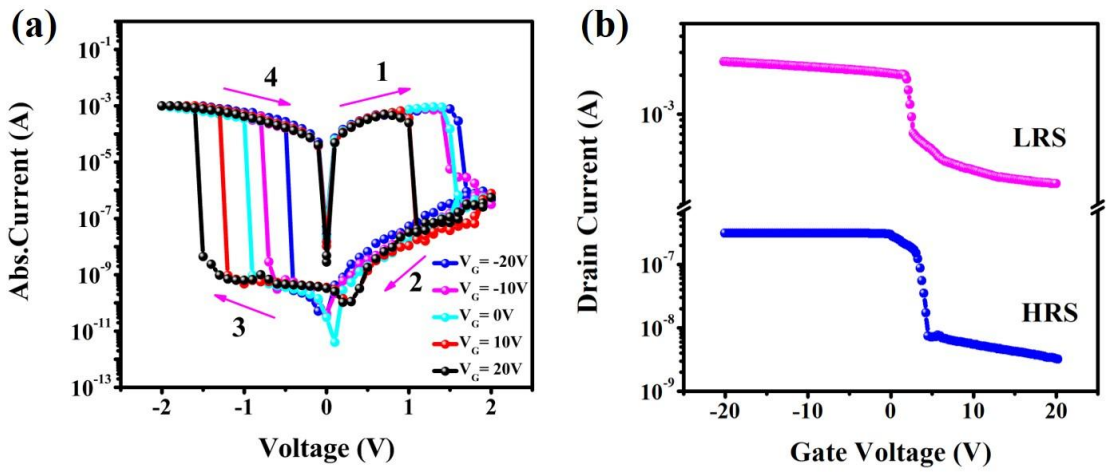

Figure 6. (a) Gate tunable resistive switching behaviors of Ag/GaSe/Ag memristor. The switching directions are denoted by the arrows. (b) Transport characteristics of GaSe-based FET at LRS and HRS.

TOC

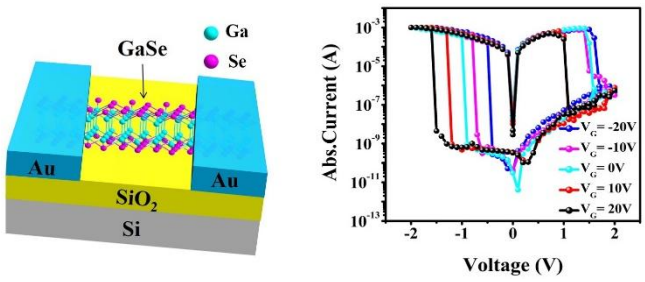
GaSe
Ga
Se
Au
Au
SiO2
Si
Abs.Current (A)
Voltage (V)
VG= -20V
VG= -10V
VG= 0V
VG= 10V
VG= 20V